Chemical Engineering & Processing: Process Intensification 189 (2023) 109383

Contents lists available at ScienceDirect

Chemical Engineering and Processing - Process Intensification

journal homepage: www.elsevier.com/locate/cep

Procedure to generate a selection chart for microwave sol-gel synthesis of nanoparticles

Paolo Veronesi [a,*], Elena Colombini [a], Özgür Sevgi Canarslan [a], Giovanni Baldi [b], Cristina Leonelli [a]

[a] Department of Engineering "Enzo Ferrari", University of Modena and Reggio Emilia, Via Vivarelli 10, 41125, Modena, Italy
[b] Ce. Ri. Col–Centro Ricerche Colorobbia Consulting, Via Pietramarina, 123, SOVIGLIANA, 50059 Vinci, Italy

ARTICLE INFO

Keywords:
Microwave synthesis
Nanotitania
Multiphysics modelling
Temperature homogeneity index

ABSTRACT

Numerical simulation is used to compare the temperature distribution existing during microwave or conventional heating by hot oil bath of a reaction volume. The simulation is applied to the sol-gel synthesis of TiO_2 nanopowders, considering temperature dependent materials parameters. A WR340-based single mode applicator operating at 2.45 GHz is considered, with a cylindrical load positioned in regions of predominant electric field. A temperature homogeneity index, defined as the ratio between the average temperature and its standard deviation at a certain time, is used to compare homogeneity of conventional and microwave heating at different power densities, from 370 to 7400 W/L. Based on that comparison, a selection chart of the more homogenous heating process as a function of power density and average temperature of the reaction volume is defined and can be used to select the experimental conditions expected to lead to a more or less homogeneous particle size of the products.

A dedicated instrumented model, including three optical fibres, is developed as well, for validation purposes. Experimental validation showed a very good predictive capability of the model, with errors on estimated temperature lower than 3 °C at temperatures lower than 80 °C.

Statement of novelty and significance

The paper describes a simple modelling-assisted method which can be useful to determine the most suitable experimental conditions to perform a microwave synthesis process, as opposed to a conventional heating one, in terms of homogeneity of temperature distribution in the reaction volume. This approach can be extended to the operation of larger microwave assisted synthesis equipment operating at the industrial scale. In this paper, this approach is applied to the sol-gel synthesis of TiO_2 nanoparticles.

1. Introduction

TiO_2 nanopowders are widely used in applications related to sustainable energy and environment, ranging from the use as membranes, sensors and photocatlysts. Their application on such fields are strictly dependent on particle size, morphology and kind of polymorph [1–4]. Nucleation and growth are governing phenomena affecting the TiO_2 nanopowders, depending on the synthetic route used. Hence, many researchers have studied the nucleation and growth kinetic of TiO_2 nanopowders, especially from aqueous solutions or by sol-gel method [5–10]. The wide majority of these studies demonstrated that the average size of primary particles depends on parameters like solution chemistry, time and temperature [11]. Being temperature distribution in the synthesis volume the main topic addressed by the present study, a more detailed overview of the effect of this parameter, as reported in literature, is beneficial.

Demopoulo et al. [12] produced e nanostructured TiO_2 particles by precipitation from forced hydrolysis of aqueous Ti(IV) chloride solution. The kinetic of such a reaction presents slow nucleation, while the growth rate is fast. These authors introduced a two-step process to describe the formation of TiO_2 nanoparticles, being the first step the nucleation and aggregation of elementary nanocrystallite (≈ 10 – 2 nm) and the second step the growth of elongated self –assembled nanofibers. The possibility

* Corresponding author.
E-mail address: paolo.veronesi@unimore.it (P. Veronesi).

https://doi.org/10.1016/j.cep.2023.109383
Received 26 January 2023; Received in revised form 14 March 2023; Accepted 16 April 2023
Available online 17 April 2023

of having separate events or conditions for nucleation and growth is mandatory to achieve careful control over the final particle size. In a recent study by Zhang [13] involving the synthesis of TiO_2 nanoparticles by hydrolysis of a titanium tetrachloride ($TiCl_4$) precursor in aqueous solution at temperature below 100 °C, the authors individuated three periods: (i) the induction, (ii) the initial growth and (iii) the saturated growth. Induction time depends on the $TiCl_4$ concentration and pH, and the effect of increasing temperature is reflected in supersaturation, which results higher as higher the temperature, $TiCl_4$ concentration and pH are. Thus, sol-gel synthesis resulted as one the best techniques that can be applied to investigate the nucleation and growth kinetic of TiO_2 nanoparticles [13]. The sol-gel process is affected by the kind of metal precursor used, pH of the solution, possible presence of catalyst and, again, temperature. In sol-gel synthesis, it is easier to control hydrolysis and polycondensation reactions, in order to achieve the required properties of the final products [14]. In particular, temperature affects the rate constant for coagulation of particles, which increases as temperature increases due to the temperature dependence of the velocity of the monomer through the particles. This effect of temperature was reported also in the kinetic growth studies performed by Jean and Ring [15], who synthesized ultra-fine and spherical of TiO_2 nanoparticles, confirming that the nucleation period was limited to a short period of time and the growth process was induced by another step. Hence, it is possible to separate the two events and use nucleation through supersaturation to produce almost perfect monodispersed particles [16]. Using the LaMer's diagram [17], the authors demonstrated that the maximum supersaturation can be reached using higher temperatures, which lead to an increase of the diffusion coefficient of monomers, resulting in a predictable earlier occurrence of nucleation and growth of particles at higher temperature.

However, all the aforementioned studies generally refer to a "synthesis temperature", assuming extremely long residence times of the reactants, or a homogeneous temperature distribution, which is not always the case in all possible synthetic routes. For instance, microwave-assisted synthesis of nanoparticles is known to reduce the processing time from hours down to minutes [18,19], with higher yields [20,21]. However, in general microwave-assisted processes are often addressed as poorly reproducible processes, and not all the authors agree on the extent of the achievable benefits [22–25]. This uncertainty on the profitable use of microwave irradiation as heating source is often due to the selection of the experimental parameters, ranging from the type of applicator to the applied power density and temperature control systems [26–28]. As a matter of fact, microwave-assisted synthesis relies on the conversion of the energy from an impinging electromagnetic field into heat in the reaction media. This conversion is dependent on the permittivity of the material exposed to the microwaves, but the heat generated, and the subsequent temperature rise, are affected by the local strength of the electromagnetic field and the heat dissipated through the reactor's walls [29]. Being heat generated directly within the load, the temperature distribution in a reactor under microwave irradiation can result quite different from that of a more conventional hot oil bath, and such difference can be responsible for experimentally observed specific effects, sometimes wrongly addressed as "microwave non-thermal effects" [30]. However, it is the electromagnetic field distribution in the microwave reactor which at its turn determines how heat is spatially generated in the reaction volume. Additionally, it is determined by the microwave source (power, spectrum, duty cycle) as well as the reactor shape and dimensions, not neglecting all auxiliaries and the load itself. As a result, in a microwave powered reactor usually large gradients of electric field strength exist, leading to localized overheating of some regions of the load which can not be compensated by heat transfer alone. Moreover, this non-uniform temperature distribution is responsible for the generation of "permittivity gradients" in the load, which further affect the electromagnetic field distribution, leading also to other unwanted phenomena like thermal runaway. Such condition is clearly visible using thermochromic materials, like the ones recently prepared by Shen et al., which confirm that the problem of uneven heating still limits the application of microwave in chemical engineering, because uneven heating of reactants gives rise to the problem of inconsistent product quality or inaccurate reaction kinetic [31]

In this framework, a recently EU-funded project, SIMPLIFY (Sonication and Microwave Processing of Material Feedstocks) [32], is investigating, amongst others, the process intensification which can evolve with the use of 2.45 GHz microwave irradiation as heating source for the synthesis of TiO_2 nanoparticle in a Plug Flow Reactor (PFR). In order to fully exploit the potentially faster synthesis of monodispersed TiO_2 nanoparticles in presence of microwaves, a deeper understanding of the temperature distribution achievable in microwave assisted reactions is mandatory, and it is the objective of this paper. The present study proposes a novel modelling-based selection of the experimental conditions in order to achieve a desirable combination of fast processing and narrow temperature distribution within the reactor when synthesizing the TiO_2 nanoparticles from alkoxide precursor hydrolysis. The sol-gel synthesis of titanium dioxide nanoparticles has been selected as the model system because it does not require complex installations and the synthesis proceeds under ambient pressure and temperature. Moreover, the sol-gel synthesis is based on the hydrolysis/condensation of a titanium precursor to produce a sol and then a gel. In our synthetic route, since the very early stage of reactants mixing, a high viscosity gel is formed and this allows to neglect convective motion inside the load, further simplifying the model. Moreover, literature results address the influence of many variables, from pH to temperature, on the final particle size of the nanoparticles, and thus such a system can be considered a good starting point to assess the effects of different temperature distributions existing in the same reaction volume, heated by different techniques.

2. Materials and methods

2.1. Chemical reaction and dielectric properties

In order to investigate the temperature distribution existing in microwave-assisted reactions in batch or flow reactors, the following reaction has been considered:

HCl

$$Ti\{OCH(CH_3)_2\}_4 + 2H_2O \rightarrow TiO_2 + 4(CH_3)_2CHOH \quad (1)$$

where reactants are titanium isopropoxide (technical grade) and a premixed aqueous HCl solution (technical grade) with a small amount of a surfactant, commercially known as Triton X-100 (Sigma Aldrich, Merk Life Science S.r.l., Milan, Italy, laboratory grade). The amounts of such reactants are:

32% HCl = 3.1%

Bi-distilled water = 96.9%

Triton X-100 = 0.013%

The synthetic route starts with pre-heated concentrated HCl, TX-100 and water, positioned in a vessel heated by means of diathermal oil circulating in the external jacket. The temperature is then raised to 40 °C and $Ti[OCH(CH_3)_2]_4$ is added very rapidly, until a white flock precipitate can be seen immediately. Starting from these conditions, further heat is supplied to the reaction vessel by diathermal oil (conventional heating) or by microwave heating, up to the target temperature of 80 °C is achieved. In the first case, heat is progressively conducted from the outer of the reactor volume to the load, while in the second case, volumetric heating occurs, depending on the permittivity of the load.

In order to investigate heating rate and temperature distribution during microwave exposure of the reactants, their permittivity has been measured in the 1–3 GHz range using an Agilent 85070E Dielectric Probe Kit (Agilent Technologies, Santa Clara, CA, USA). The measurements have been performed while heating the reactants mixture by hot water and monitoring the temperature by an optical probe (Neoptix T1

Fig. 1. measurement device for temperature dependent permittivity of liquids. From the top: cover with holes for insertion of temperature sensor and O-ring (not visible), heating/cooling jacket with inlet and outlet ports, truncated co-axial probe (from Agilent Dielectric Probe kit), O-ring and holding base.

Optic Temperature Probe, Neoptix, Quebec City, Canada) in the range 25–80 °C. Temperature dependent permittivity has then been expressed by interpolating the measured data, as reported elsewhere [32], leading to the following expression:

$$\varepsilon(\mathrm{T}) = (-0.06 * \mathrm{T} + 72.589) - \mathrm{i} * (0.15 * \mathrm{T} - 22.975) \quad (2)$$

Fig. 1 depicts the setup used to measure permittivity, which at a later stage was used also to validate the numerical simulation results.

2.2. Microwave reactors

A small single mode reactor (batch system), based on WR340 waveguide, operating at the nominal ISM frequency of 2.450 GHz has been simulated. A modified version of this applicator, including the presence of three optical fibres for temperature sensing has been modelled as well. This applicator has been used to validate modelling results, and served for the design and development of a larger one [33], which is currently used for the laboratory scale production of TiO_2 nanoparticles at CE.RI.COL. Labs (Italy).

Numerical simulation (see next paragraphs) has been conducted by FEM using COMSOL MultiPhysics software, setting the coupling of predefined application modes of RF and heat transfer, neglecting fluid flow. This allows a two way coupling of the electromagnetic field and the thermal field, being their effect superimposed and affected by each other. As a matter of fact, permittivity of the reactive mixture, hereafter indicated as “load”, affects the electromagnetic field distribution in the applicator, which at its turn affects the heat generation within the load, and, hence, the temperature of the load raises with subsequent changes of permittivity. Neglecting to do so, in rapid heating conditions, could lead to macroscopic underestimate of the effective temperature in the load [34].

The simulated reactor has been assembled and tested, and used to validate the modelling results by continuous temperature measurements on a cross section of the load. Temperature was measured in three different points on the same horizontal section using optical probes (Neoptix T1 Optic Temperature Probe, Neoptix, Quebec City, Canada). Such probes are non-metallic and hence induce a small perturbation of the electromagnetic field in the reactor; however, their size and heat capacity is not negligible compared to the load, especially when it comes to the effects on temperature. For this reason the aforementioned modified model has been developed. During validation, a LEANGEN-2450M-250-E solid state source (LEANFA Srl, Ruvo di Puglia, Italy) operating at 2.45 GHz has been used for its capabilities of carefully controlling the emitted power at 1 W steps, measuring the reflected power, and its narrow bandwidth which is much more similar to the simulated source than a conventional magnetron-based source is.

2.3. Model definition

A simple geometry, namely a portion of a rectangular waveguide of the WR340 type (86 mm x 43 mm cross section dimension), terminated on one side by a shorting movable plunger and on the other side

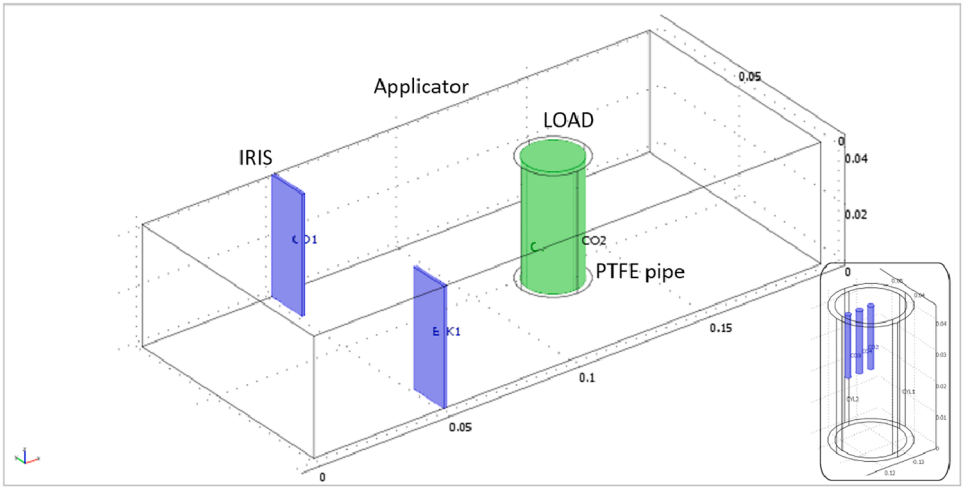

Fig. 2. model geometry, showing the load (reactants, in green) contained in the PTFE pipe (transparent) and the coupling iris (blue), in the single mode applicator. In the box, an alternative load geometry, with three optical fibres inserted is shown in blue colour. Numbers indicate dimensions in metres. A detailed description of the model geometry is supplied as supplementary content.

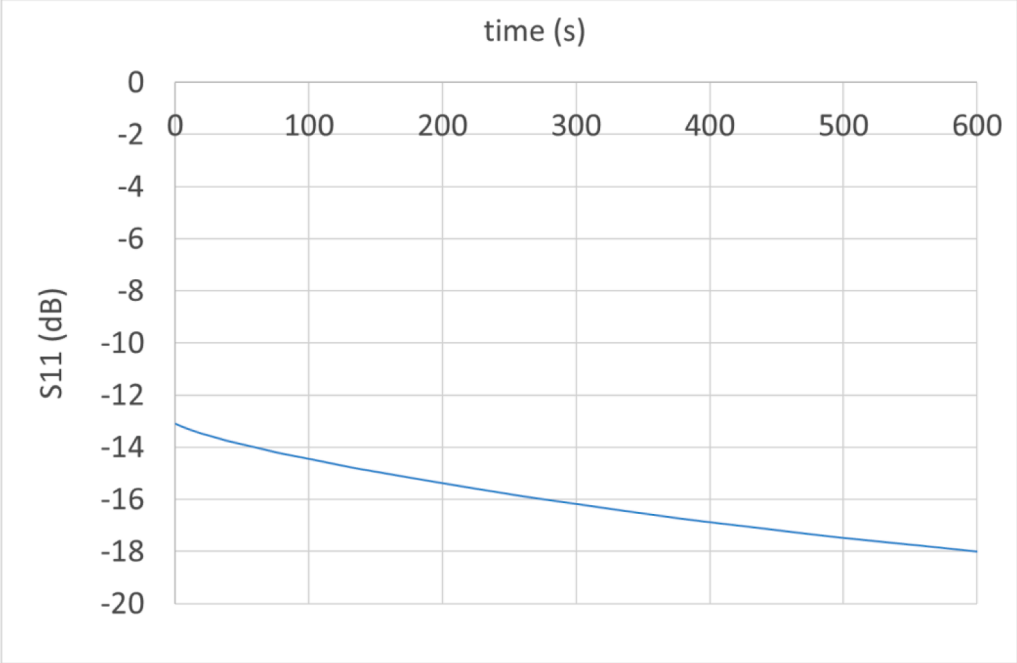

Fig. 3. Reflection coefficient at 2.45 GHz as a function of the heating time for an incident power of 10 W.

connected to a microwave generator, with interposed a coupling iris, has been used to simulate the temperature distribution existing during the microwave-assisted synthesis of TiO_2 nanoparticles. The load consists of a PTFE pipe, 43 mm height, 20 mm of internal diameter and 2 mm thick, containing the reactants. Fig. 2 depicts the model geometry.

The predefined application mode of microwave heating of COMSOL 3.5 was used, as it already implements a two way coupling between electromagnetic field, generating the proper power density, and heat transfer, with subsequent temperature modification of the load. The microwave generator was simulated by a boundary condition exciting the input port at 2.45 GHz in the TE01 mode, while the remaining boundaries were considered as perfect electric conductors, including the iris. The input power was varied from 5 to 100 W. The load permittivity was set as temperature dependent according to the interpolating Eq. (2), while the PTFE pipe is assumed with a constant permittivity of 2.1-i*0.004 [35].

The load thermal properties like density and heat capacity were considered temperature independent for the simplicity's sake, while the thermal conductivity was based on literature data on similar water-nanoparticles system, with a small volume fraction of nanoparticles, and were assumed as:

Density: 1096 kg/m^3

Thermal conductivity: $0.001*T + 0.527$ W/mK [36]

Heat capacity: 720 J/kg*K [37]

The latter value, heat capacity, has been selected as a starting point, then further refined by comparing the numerical simulation results of the conventional heating (see end of this chapter) to the experimental results. This allowed us to achieve a more reliable prediction of temperature distribution, being the literature value referred to a slightly different reaction path and volumetric fraction of nanoparticles.

For the PTFE pipe, values from the COMSOL database of 2100 kg/m^3 for density, 0.25 W/mK for thermal conductivity and 1100 J/kgK for heat capacity have been assumed.

Two kinds of boundary conditions have been set: for conventional heating by hot oil bath: a constant temperature set at the PTFE outer walls of 80 °C, to simulate the direct exposure to the hot oil bath; for microwave heating: a temperature of 30 °C at the PTFE outer walls, with a heat transfer coefficient of 1.6 W/m^{2}K, to simulate the microwave heating in the reactor at room temperature. In this case, also a volume heat generation term amounting to the power density generated in the load by the electromagnetic field was introduced, to achieve the two way coupling of the RF and thermal application modes of Comsol.

In this simplified model, no convection has been considered, assuming that the fluid is static and not stirred, hence not subjected to any shear rate. In these conditions, a high viscosity of the sol-gel system is expected [38].

A further variation of this model has been introduced to simplify the subsequent experimental validation, namely placing three probes (optical fibres) at three different radial positions in the load, 20 mm from the top surface. The small box of Fig. 2 shows the modified geometry of the load with the three probes inserted. The probes are PTFE coated and are simulated here having the dielectric and thermal properties of silica glass [38,39]. This model, and the applicator which was used for the validation, is here used also to refine the heat capacity values, by comparing the experimental temperature profiles with the modelling results deriving from a parametric model where load heat capacity have been varied within a predefined range centred on literature values. This preliminary modelling activity, to reconstruct average thermal parameters under conventional heating conditions, is then extended to the microwave heating case.

The numerical simulation was conducted using COMSOL Multiphysics software, with a time dependent direct solver, limiting the duration of the simulation to the achievement of an average temperature of the load of 80 °C, i.e. within the experimentally measured temperature- dependent permittivity values.

3. Results

Numerical simulation results will be presented separately for the case of the temperature sensor-free case and for the case which will be used for validation.

3.1. Numerical simulation of single mode reactor

A preliminary optimization on the plunger position was performed in order to find the conditions of minimum reflected power. Fig. 3 shows the variation of the reflection coefficient as a function of time, in the optimized conditions. Results indicate that the reflected power is always

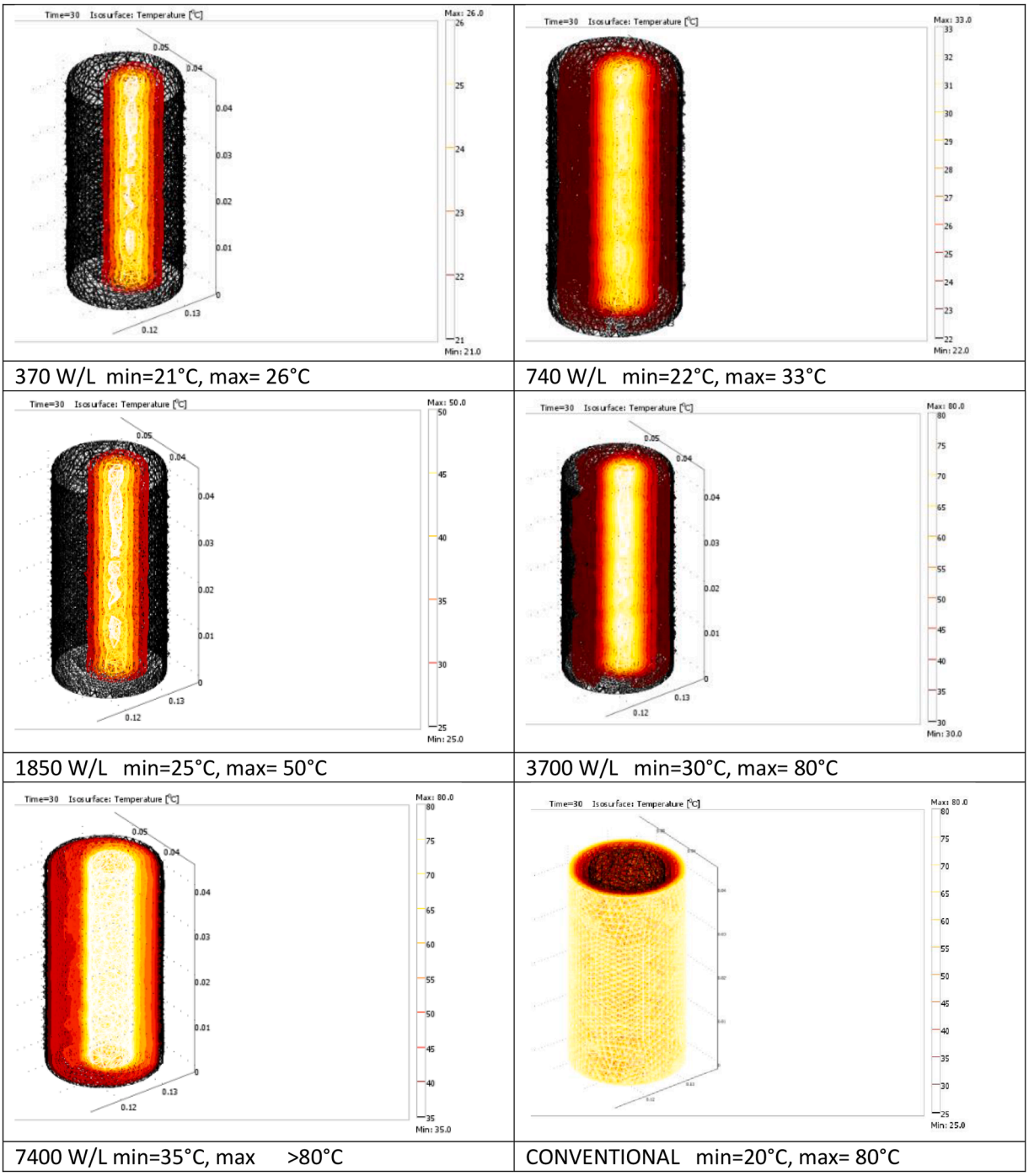

Fig. 4. Temperature distribution after 30 s of microwave heating at the indicated power density and with number referring to the minimum and maximum temperature in the temperature scale used to represent the plots and comparison with conventional heating. Animations showing as temperature slice plots the whole heating are available as supplementary files.

lower than 5% and it tends to decrease to less than 2% as the load is progressively heated in time, and hence it changes its permittivity. Assuming that the power dissipated in the PTFE pipe is almost negligible, due to its almost lossless nature, according to the model that we developed, we used the complement to 100% of the simulated reflected power to define the power dissipated on the load. Thus, a reference power density in the load is defined by dividing such value by the load volume and it is used to compare different scenarios.

As a matter of fact, numerical simulation of the fully coupled model is here used mainly to investigate possible differences in the temperature distribution in the load as a function of the power density (370, 740, 1850, 3700, and 7400 W/L) on the load, i.e. a section of the PTFE pipe. Power density has been expressed in terms of Watts per unit volume in litres, being this quantity immediately transferrable to the laboratory practice. Fig. 4 shows the temperature distribution in the load (PTFE pipe+ reactants) existing after 30 s of heating, compared also to conventional heating. For the clarity's sake, a different temperature scale has been used in the figures and it is indicated in the captions, whilst colours have been chosen from red to white with increasing temperature.

It is evident how the use of microwaves induces a higher temperature in the central parts of the load (brighter area), while in conventional

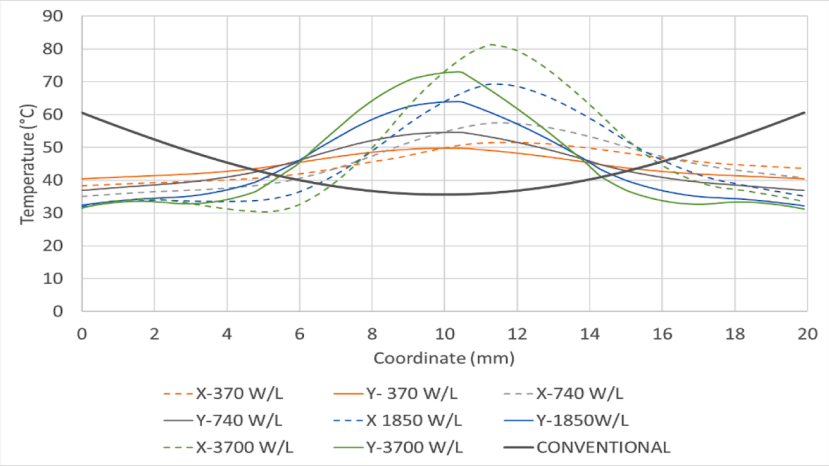

Fig. 5. Temperature profiles for an average load temperature of 45 °C along two perpendicular segments passing through the midpoint of the reactants (i.e. not including the PTFE pipe) in case of microwave heating at different power density, compared to conventional heating. Dashed line are referred to segments orientated along the X axis, while continuous lines are referred to the Y axis.

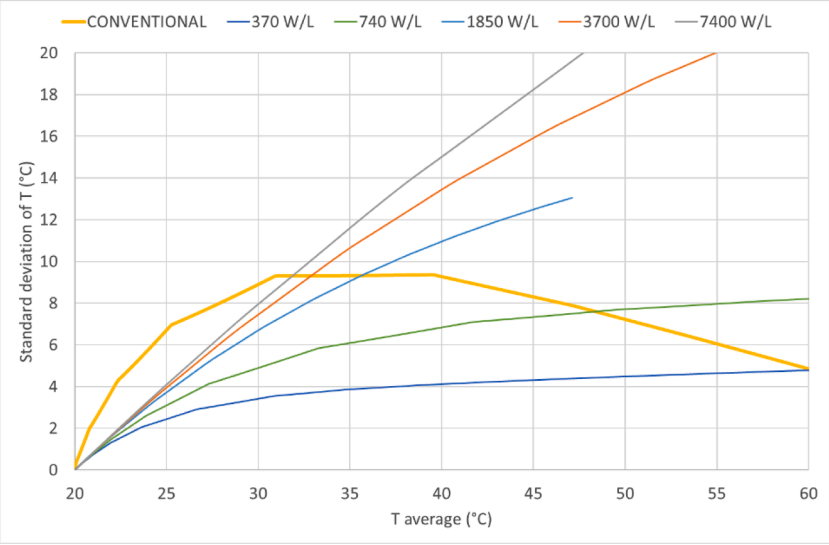

Fig. 6. Standard deviation of temperature distribution along a longitudinal cross section of the reactants (i.e. not including the PTFE pipe) as a function of the average temperature in case of microwave heating at different power density compared to conventional heating.

heating the walls exposed to the 80 °C environment are heated first. This rather obvious result, however, allows to gather a deeper understanding on the possibility to run microwave-assisted reactions with a completely different temperature distribution in the reaction volume, once the proper geometry of the sample and the microwave reactor has been designed.

Numerical simulation allows us to estimate temperature in each portion of the volume, and in this study it is used to identify the experimental conditions leading to a different degree of temperature homogeneity, compared to conventional heating. To do so, the temperature distribution along two perpendicular directions, parallel to the X and Y axis and passing through the mid height of the load has been evaluated every 0.1 mm, leading to the temperature profiles shown in Fig. 5. All these curves have been referred to as the conditions of load average temperature equal to 45 °C.

Fig. 5 shows that, despite the average temperature of 45 °C, in case of microwave heating at high power density, temperatures exceeding 80 °C can be found. The same does not happen in case of conventional heating, being the $T = 80$ °C the condition set on the external surface of the PTFE container.

The plot of Fig. 5 allows also to estimate how broad is the temperature distribution along the investigated directions by simply considering the extension of each curve along the ordinate axis. Hence, results show also that in the simulated conditions the temperature distribution in case of microwave heating results broader along the X direction, compared to the Y one (symmetry axis of the model).

A further additional result derived from Fig. 5 is that under relatively low power density, the temperature distribution in case of microwave heating can be more homogenous than in case of conventional heating. In order to better evidence this specific feature, the temperature has been evaluated also along a longitudinal cross section, parallel to the axis of the applicator, every 1 mm spacing, and the standard deviation of such temperature distribution has been calculated, together with the average value of the temperature. The standard deviation is assumed as an indication of how homogenous the temperature distribution is, the average temperature is taken as an indication of how rapidly the heating occurs. Fig. 6 plots the results of such calculations for the same conditions investigated above.

The intersection of the conventional heating curve with the microwave heating one defines the locus of points (T*) below which

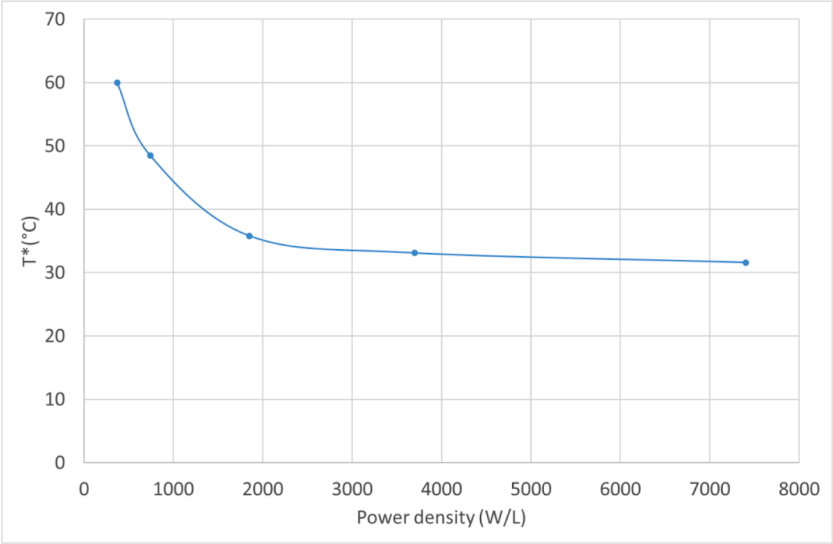

Fig. 7. T* temperature as a function of the microwave power density. (For the definition of T*, see the text).

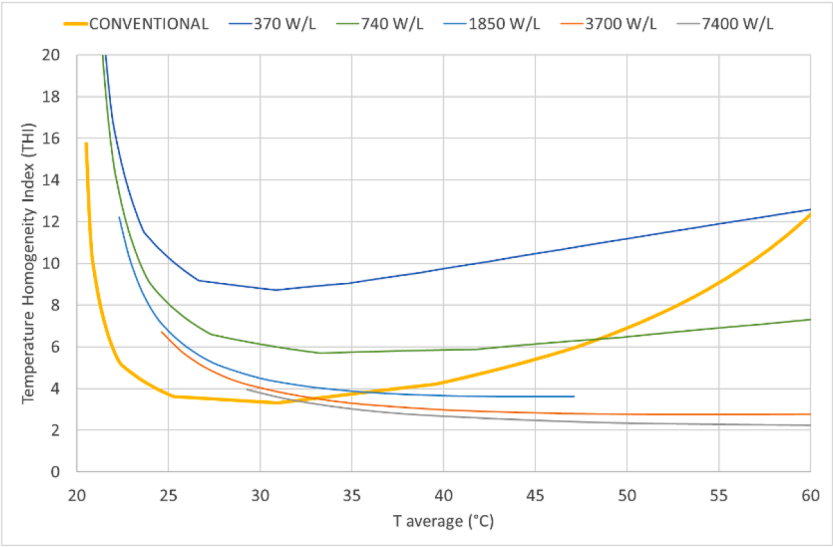

Fig. 8. Calculated temperature homogeneity as a function of the average temperature, for different microwave power density and comparison to conventional heating.

microwave heating results in a narrower temperature distribution compared to conventional heating, limited to the simulated conditions. Fig. 7 summarizes this locus, where T* indicates the average temperature at which the standard deviation of the temperature obtained by microwave heating is identical to the one obtained by conventional heating.

Such a plot can be particularly useful for deciding the experimental setup leading to some wanted results. For instance, in case of classical nucleation and growth, a narrower temperature distribution can be helpful in having a controlled (and rapid) nucleation and subsequently, increasing temperature, moving to the growth phase, if required. Such conditions should lead to a better control of particle size during nanoparticle synthesis. On the other hand, a broader temperature distribution can lead to the condition of nucleation and growth occurring simultaneously, leading to a presumably broader particle size distribution of the synthesised nanopowders.

Furthermore, if it is desirable to reach high temperature in very small portions of the load, for instance to locally reach activation energies while the reactants remain at an average lower temperature (the so called "hot spots" [40–42]), it is preferable to operate by microwaves in the region above the line of Fig. 7.

Thus, Fig. 7 can be considered as a modelling-based selection chart for the experimental conditions, so that the researcher can know in advance if the applied conditions (power density, in this case) will lead to a narrower (region below the line of Fig. 7) or to a broader (region above the aforementioned line) temperature distribution.

In the investigated conditions, where the objective of the synthesis is to achieve a monodispersed and fine TiO_2 nanoparticles suspension, Fig. 7 suggests to use extremely low microwave power densities if the synthesis has to be carried out at temperature in excess of 60 °C, otherwise the use of conventional heating is preferable.

A further elaboration of the presented data allows to have an immediate quantification of the desirability of a certain experimental setup, by defining a temperature homogeneity index (THI) as the ratio between the average temperature and its standard deviation at a certain time ($THI=T_{avg}/\sigma(T)$). A high value of such a ratio indicates rapid and homogenous heating. Fig. 8 shows the trend of the temperature homogeneity index as a function of the average temperature of the reactants.

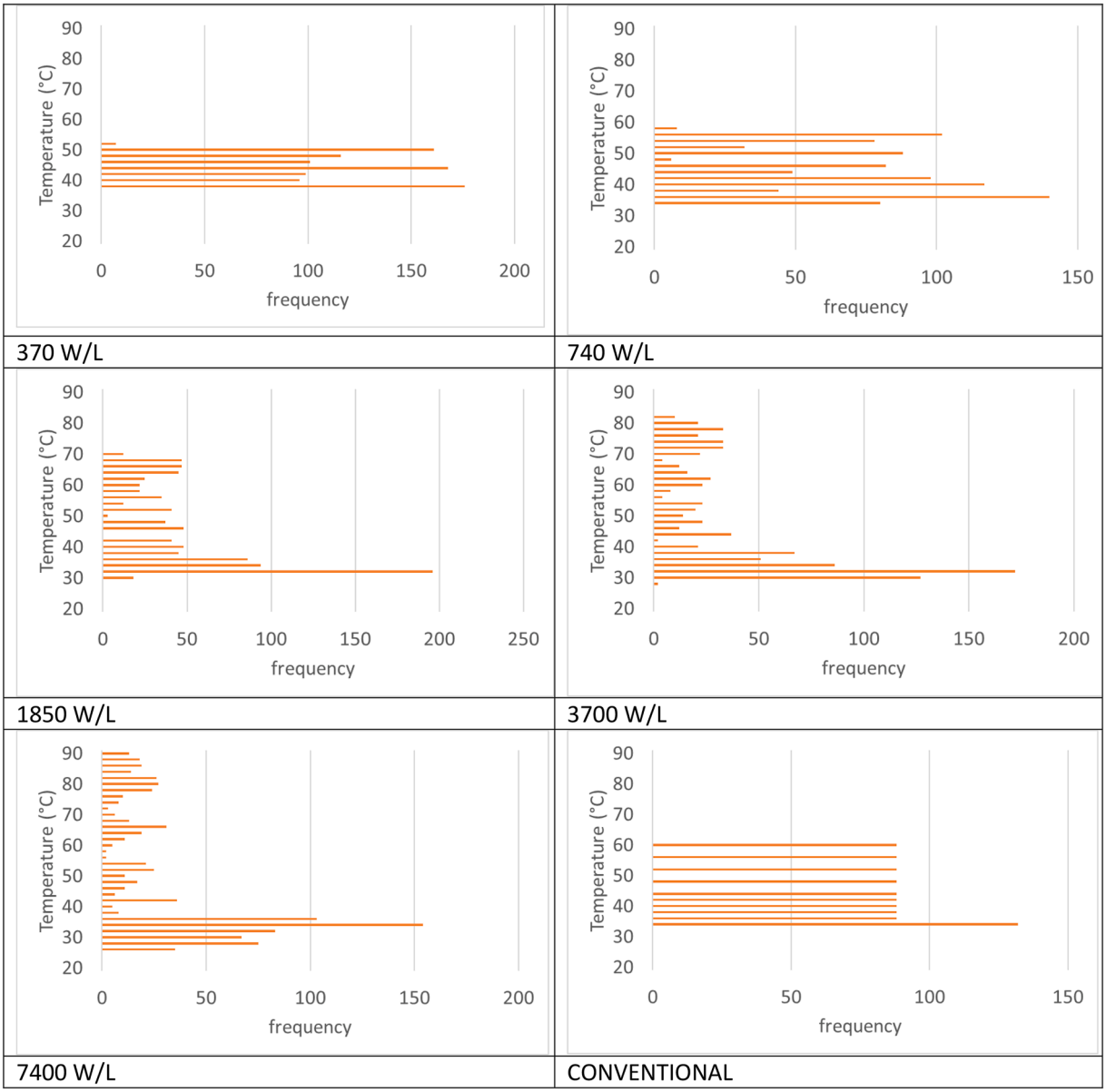

Fig. 9. Distributive curves of temperature in a longitudinal cross section of the reactants, for an average temperature of 45 °C, as a function of the microwave power density and compared to conventional heating.

As expected, the lower power density, implying also longer heating times, leads to higher values of the THI, because in such conditions heat transfer helps homogenise the temperature distribution induced by the microwave heating (which is localized in the centre, as previously shown in Fig. 4).

In order to better clarify the importance of selecting the proper power density level, an additional elaboration of the simulated data can be made considering the distributive curve of temperature at a given average temperature. Fig. 9 shows such calculations in the longitudinal cross section of the load at an average temperature of 45 °C.

Results of Fig. 9 demonstrate once more how the use of microwave heating at low power density, in the simulated conditions, can lead to a much narrower temperature distribution. It also confirms that at a given average temperature, in case of microwave heating, there can exist regions at extremely different temperatures, like in the case with maximum power density, reaching up to 90 °C.

Whether it is most desirable achieving a high temperature homogeneity in the reaction volume or, vice versa, favouring the formation of hot spots, it is strictly dependent on the type of synthesis considered and how nucleation and growth curves are superimposing at certain temperatures. In case of nanoparticles synthesis, the generation of hot spots could locally facilitate mass transfer and chemical process efficiency, but at the cost of reproducibility, as the generation of hot spots is still not controllable a priori. On the other hand, the presence of reaction environments with extremely controlled and homogenous temperatures is expected to enhance selectivity amongst competing processes requiring different activation energies or temperatures. In this framework, the possibility of creating process maps is helpful in setting up the most promising experimental conditions to trigger a desired temperature-related effect.

3.2. *Numerical simulation of instrumented small single mode reactor*

In order to validate the numerical simulation results, a more detailed model has been used, including the presence of three optical fibres for temperature monitoring, as shown in the box of Fig. 2. The presence of such fibres induce small changes in the electromagnetic field distribution, but, most importantly, affect the temperature profile. This effect is

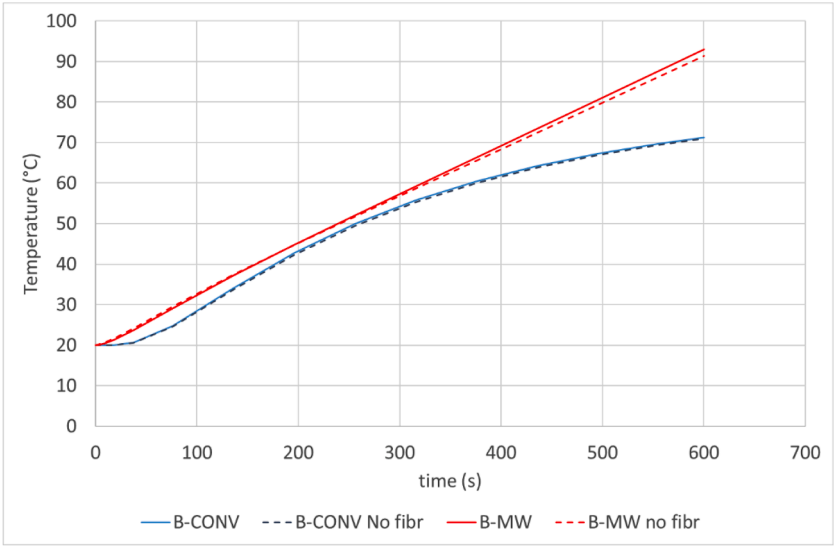

Fig. 10. temperature vs time curves in the second temperature probe position, in the box of Fig. 2, in case of microwave (MW) or conventional (CONV) heating, with or without (no fibr) considering the probes' presence.

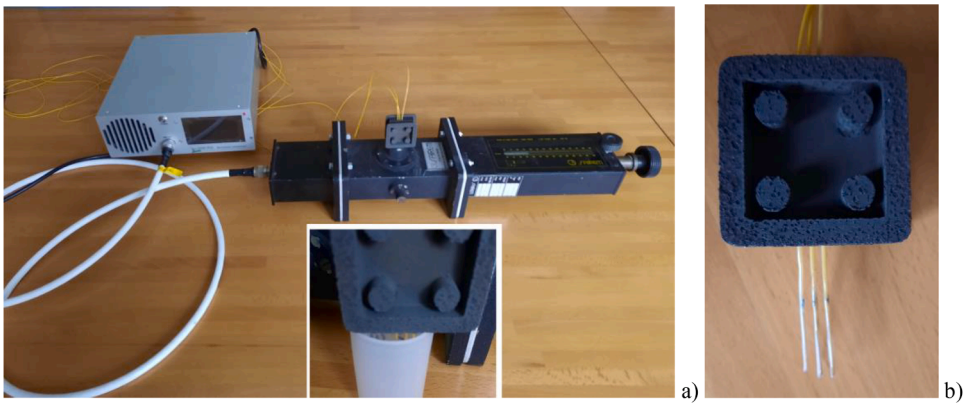

Fig. 11. Experimental setup used for validation: a) microwave apparatus: from the left: 1-solid state microwave generator, 2-coaxial cable, 3-coaxial to waveguide transition, 4-coupling iris, 5-applicator with probes inserted, 6-shorting plunger. In the box: probes inserted in the load; b) Probes and holding fixture.

ascribable not only to the heat capacity of the fibres, but also to the fact that the presence of the fibres corresponds to a lower volume of the load. For this reason, in the microwave heating models of the instrumented reactor, we re-scaled the emitted power by the simulated microwave source in order to achieve identical power densities with respect to the not instrumented case. Fig. 10 shows a comparison between the two models, where power density is set to identical (740 W/L). The "no fibr" suffix indicates the results in absence of the fibres.

The differences, even if relatively small and lower than 2 °C after 600 s heating, are more significant in case of microwave heating. Thus,

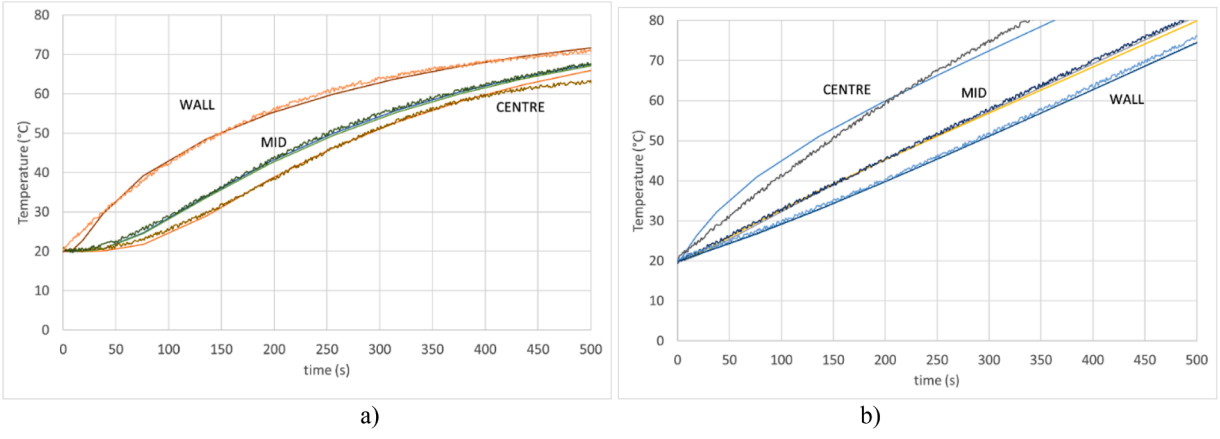

Fig. 12. Measured (dotted line) and simulated (continuous line) heating curves in case of: a) conventional heating, b) microwave heating at 740 W/L power density.

the data obtained for the instrumented model have been used for the comparison with the experimentally measured one.

3.3. Validation

Fig. 11 shows the experimental apparatus used and the probe arrangement, including the fixture used to hold the probes at the proper position inside the load.

The equipment shown in Fig. 1 has been used for the validation of the conventional heating results, using the same probe arrangement and fixture of Fig. 11b. Three repetitions have been made and the average value of temperature was taken as the experimental value.

Fig. 12 shows the simulated and measured temperature vs time curves, for the three measurement points, indicated as "CENTRE"= probe in the centre of the load, "MID"= probe 4 mm radially distant from the previous one, "WALL"= probe set near the reactor walls, at 8 mm from the first one.

Results show a very good agreement between the performed measurements and the simulated ones, especially in case of conventional heating. This was to be expected because the conventional heating experimental curve in the midpoint was used to refine the model thermal properties, as described earlier, and it is obviously reflected also on the other measuring points. The largest deviation from the experimental measurements occurs in the "CENTRE" probe, but it is still limited to less than 3 °C. Comparing the MID probe measurements, from time=400 s, the centre of the load seems to reduce its heating rate more than the other points. This rather unexpected value, which has been encountered in all the three sets of measurements performed, will be subject of further investigations, but led the authors to limit the discussion of the temperature homogeneity only within the validated temperature range, i.e. 60 °C, as shown in Figs. 6-8.

A larger deviation, but still lower than 4 °C, is encountered in case of microwave heating, and this can be explained both considering that the model neglects convection and that it assumes an external constant temperature outside the PTFE pipe. Moreover, the optical fibres have a thin PTFE coating, neglected in the model. It is also evident that the model deviations from the experimental results tend to increase as temperature increases, and this is due to the fact that the interpolating function for dielectric properties of reactants is based on measurements of permittivity up to 80 °C, so extrapolation outside this range could be prone to errors. This is the reason why the graphs of Fig. 12 have been truncated at 80 °C temperature.

Nevertheless, the most important validated result is that the experimental system is able to appreciate temperature differences occurring during the first 500 s of heating, and that such differences are in very good agreement with the simulated ones.

4. Conclusions

The sol-gel synthesis of TiO_2 nanoparticles has been investigated by numerical simulation, in order to identify the most suitable conditions leading to the control of the nanoparticles size and homogeneity of particle size distribution in case of microwave-assisted synthesis. Numerical simulation allowed us to estimate temperature distribution in microwave heated reactors and to compare it with conventionally heated ones. An instrumented model was developed to refine the thermal parameters of the model and for subsequent validation of the modelling results. Validation, both of the microwave heating and conventional heating condition, shows a very good agreement between experimental and simulated heating curves of three different points in the load, 4 mm spaced.

The validated model has been used to investigate the existing temperature distribution during the sol gel synthesis, leading to the development of a process conditions selection chart, which can be used as a guideline to perform microwave synthesis with maximum or minimum temperature distribution homogeneity. Depending on the desired results, i.e. rapid nucleation of nanoparticles occurring homogeneously in the load volume or generation of localized hot spots, the proposed modelling-based approach can serve to determine the most suitable power density in a given microwave reactor to achieve one such two conditions. Despite being a simplified model that neglects convection due to the specific sol-gel conditions applied, the results obtained on the small single mode applicator served to develop a larger prismatic applicator, which has been designed accordingly and built. The details on the applicator geometry and the applied modelling strategy is described in a recent paper by the authors [33]. This resulted in the possibility to run the synthesis continuously. The scale up of such a continuous process at industrial scale should see microwave irradiation to generate a very rapid heating within the reaction volume, while keeping a satisfactory temperature homogeneity. The implementation of such a process is one of the future targets of this investigation.

Declaration of Competing Interest

The authors declare the following financial interests/personal relationships which may be considered as potential competing interests:

Paolo Veronesi reports financial support was provided by European Union. Paolo Veronesi reports equipment, drugs, or supplies was provided by LEANFA Srl.

Data availability

Data will be made available on request.

Acknowledgements

The authors would like to thank LEANFA Srl for providing the microwave solid state generator used during tests

Funding

This work was carried out in the context of a larger European project named: "Sonication and Microwave Processing of Material Feedstock (SIMPLIFY)" supported by the European Union's Horizon 2020 research and innovation program under Grant Agreement No 820716.

Supplementary materials

Supplementary material associated with this article can be found, in the online version, at doi:10.1016/j.cep.2023.109383.

References

[1] J. Shi, S. Shang, L. Yang, J. Yan, Morphology and crystalline phase-controllable synthesis of TiO2 and their morphology-dependent photocatalytic properties, J. Alloys Compd. 479 (2009) 436–439, https://doi.org/10.1016/J.JALLCOM.2008.12.107.

[2] X. Chen, S.S. Mao, Titanium dioxide nanomaterials: synthesis, properties, modifications, and applications, Chem Rev 107 (2007) 2891–2959, https://doi.org/10.1021/cr0500535.

[3] M.A. Behnajady, N. Modirshahla, M. Shokri, H. Elham, A. Zeininezhad, The effect of particle size and crystal structure of titanium dioxide nanoparticles on the photocatalytic properties, J. Environ. Sci. Health A 43 (2008) 460–467, https://doi.org/10.1080/10934520701796267.

[4] M. Ni, M.K.H. Leung, D.Y.C. Leung, K. Sumathy, An analytical study of the porosity effect on dye-sensitized solar cell performance, Solar Energy Mater. Solar Cells 90 (2006) 1331–1344, https://doi.org/10.1016/J.SOLMAT.2005.08.006.

[5] V.G. Courtecuisse, K. Chhor, J.F. Bocquet, C. Pommier, Kinetics of the titanium isopropoxide decomposition in supercritical isopropyl alcohol, Ind. Eng. Chem. Res. 35 (1996) 2539–2545, https://doi.org/10.1021/IE950584R/ASSET/IMAGES/MEDIUM/IE950584RE00016.GIF.

[6] I.C. Baek, M. Vithal, J.A. Chang, J.H. Yum, M.K. Nazeeruddin, M. Grätzel, Y. C. Chung, S. il Seok, Facile preparation of large aspect ratio ellipsoidal anatase TiO2 nanoparticles and their application to dye-sensitized solar cell, Electrochem. Commun. 11 (2009) 909–912, https://doi.org/10.1016/J.ELECOM.2009.02.026.

[7] S.J. Kim, S.D. Park, Y.H. Jeong, S. Park, Homogeneous precipitation of TiO2 ultrafine powders from aqueous TiOCl2 solution, J. Am. Ceram. Soc. 82 (1999) 927–932, https://doi.org/10.1111/J.1151-2916.1999.TB01855.X.
[8] H. Jia, Z. Zheng, H. Zhao, L. Zhang, Z. Zou, Nonaqueous sol–gel synthesis and growth mechanism of single crystalline TiO2 nanorods with high photocatalytic activity, Mater. Res. Bull. 44 (2009) 1312–1316, https://doi.org/10.1016/J.MATERRESBULL.2008.12.016.
[9] Y. Gao, Y. Masuda, W.S. Seo, H. Ohta, K. Koumoto, TiO2 nanoparticles prepared using an aqueous peroxotitanate solution, Ceram. Int. 30 (2004) 1365–1368, https://doi.org/10.1016/J.CERAMINT.2003.12.105.
[10] T. Nishide, F. Mizukami, Effect of ligands on crystal structures and optical properties of TiO2 prepared by sol–gel processes, Thin Solid Films 353 (1999) 67–71, https://doi.org/10.1016/S0040-6090(99)00430-7.
[11] H. Mehranpour, M. Askari, S. Ghamsari, Nucleation and growth of TiO2 nanoparticles, in: M.M. Rahman (Ed.), Nucleation, InTech, 2011, pp. 1–26, https://doi.org/10.5772/25912.
[12] C. Charbonneau, R. Gauvin, G.P. Demopoulos, Nucleation and growth of self-assembled nanofibre-structured rutile (TiO2) particles via controlled forced hydrolysis of titanium tetrachloride solution, J. Cryst. Growth 312 (2009) 86–94, https://doi.org/10.1016/J.JCRYSGRO.2009.09.033.
[13] G. Zhang, B.K. Roy, L.F. Allard, J. Cho, Titanium oxide nanoparticles precipitated from low-temperature aqueous solutions: I. Nucleation, growth, and aggregation, J. Am. Ceram. Soc. 91 (2008) 3875–3882, https://doi.org/10.1111/J.1551-2916.2008.02781.X.
[14] Z. Jing, X. Qian, L. Meijun, F. Zhaochi, L. Can, UV Raman spectroscopic study on TiO2. II. Effect of nanoparticle size on the outer/inner phase transformations, J. Phys. Chem. C 113 (2009) 1698–1704, https://doi.org/10.1021/JP808013K/SUPPL_FILE/JP808013K_SI_001.PDF.
[15] J.H. Jean, T.A. Ring, nucleation and growth of monosized TiO2 powders from alcohol solution, Langmuir 2 (1986) 251–255. https://pubs.acs.org/sharingguidelines (Accessed 20 January 2023).
[16] M. Keshmiri, T. Troczynski, Synthesis of narrow size distribution sub-micron TiO2 spheres, J. Non Cryst. Solids 311 (2002) 89–92, https://doi.org/10.1016/S0022-3093(02)01607-1.
[17] C.B. Whitehead, S. Özkar, R.G. Finke, LaMer's 1950 model of particle formation: a review and critical analysis of its classical nucleation and fluctuation theory basis, of competing models and mechanisms for phase-changes and particle formation, and then of its application to silver halide, semiconductor, metal, and metal-oxide nanoparticles, Mater. Adv. 2 (2021) 186–235, https://doi.org/10.1039/D0MA00439A.
[18] Y.J. Zhu, F. Chen, Microwave-assisted preparation of inorganic nanostructures in liquid phase, Chem. Rev. 114 (2014) 6462–6555, https://doi.org/10.1021/CR400366S/ASSET/IMAGES/MEDIUM/CR-2013-00366S_0044.GIF.
[19] P.S. Shen, C.M. Tseng, T.C. Kuo, C.K. Shih, M.H. Li, P. Chen, Microwave-assisted synthesis of titanium dioxide nanocrystalline for efficient dye-sensitized and perovskite solar cells, Solar Energy 120 (2015) 345–356, https://doi.org/10.1016/J.SOLENER.2015.07.036.
[20] Y. Wang, W. Sun, H. Li, Microwave-assisted synthesis of graphene nanocomposites: recent developments on lithium-ion batteries, Rep. Electrochem. 1 (2015), https://doi.org/10.2147/RIE.S65118.
[21] A.K. Singh, U.T. Nakate, Photocatalytic properties of microwave-synthesized TiO 2 and ZnO nanoparticles using malachite green dye, J. Nanopart. (2013) 2013, https://doi.org/10.1155/2013/310809.
[22] C.H. Chan, N.I. Ab Manap, N.S.M. Nek Mat Din, A.S. Ahmad Hazmi, K.W. Kow, Y. K. Ho, Strategy to scale up microwave synthesis with insight into the thermal and non-thermal effects from energy-based perspective, Chem. Eng. Process. 168 (2021), 108594, https://doi.org/10.1016/J.CEP.2021.108594.
[23] S. Horikoshi, N. Serpone, On the influence of the microwaves' thermal and non-thermal effects in titania photoassisted reactions, Catal. Today 224 (2014) 225–235, https://doi.org/10.1016/J.CATTOD.2013.10.056.
[24] M. Al-Harahsheh, S. Kingman, S. Bradshaw, The reality of non-thermal effects in microwave assisted leaching systems? Hydrometallurgy 84 (2006) 1–13, https://doi.org/10.1016/J.HYDROMET.2006.03.056.
[25] A. Shazman, S. Mizrahi, U. Cogan, E. Shimoni, Examining for possible non-thermal effects during heating in a microwave oven, Food Chem. 103 (2007) 444–453, https://doi.org/10.1016/J.FOODCHEM.2006.08.024.
[26] R. Rosa, L. Trombi, P. Veronesi, C. Leonelli, Microwave energy application to combustion synthesis: a comprehensive review of recent advancements and most promising perspectives, Int. J. Self-Propagat. High-Temp. Synth. 26 (2017) 221–233, https://doi.org/10.3103/S1061386217040057/METRICS.
[27] G.S.J. Sturm, G.D. Stefanidis, M.D. Verweij, T.D.T. van Gerven, A.I. Stankiewicz, Design principles of microwave applicators for small-scale process equipment, Chem. Eng. Process. 49 (2010) 912–922, https://doi.org/10.1016/J.CEP.2010.07.017.
[28] R. Rosa, E. Ferrari, P. Veronesi, From field to shelf: how microwave-assisted extraction techniques foster an integrated green approach. Emerging Microwave Technologies in Industrial, Agricultural Medical and Food Processing, 2018, pp. 179–203, https://doi.org/10.5772/intechopen.73651.
[29] C. Leonelli, P. Veronesi, Microwave reactors for chemical synthesis and biofuels preparation, Prod. Biofuels Chem. Microwave (2015) 17–40, https://doi.org/10.1007/978-94-017-9612-5_2.
[30] D.A.C. Stuerga, P. Gaillard, Microwave athermal effects in chemistry: a myth's autopsy: part ii: orienting effects and thermodynamic consequences of electric field, J. Microwave Power Electromagn. Energy 31 (2016) 101–113, https://doi.org/10.1080/08327823.1996.11688300.
[31] Xi Shen, Hong Li, Zhenyu Zhao, Xingang Li, Kai Liu, Xin Gao, Imaging of liquid temperature distribution during microwave heating via thermochromic metal organic frameworks, Int. J. Heat Mass Transf. 189 (2022), 122667, https://doi.org/10.1016/j.ijheatmasstransfer.2022.122667.
[32] SIMPLIFY - Sonication and Microwave Processing of Material Feedstock; Grant agreement No° 820716; Start Date: 1.11.2018, End Date: 20.04.2023; https://cordis.europa.eu/project/id/820716, (n.d.).
[33] G. Poppi, E. Colombini, D. Salvatori, A. Balestri, G. Baldi, C. Leonelli, P. Veronesi, A multi-physic modelling insight into the differences between microwave and conventional heating for the synthesis of TiO2 nanoparticles, Processes 10 (2022) 697, https://doi.org/10.3390/PR10040697/S1.
[34] E. Colombini, R. Rosa, P. Veronesi, A. Casagrande, Memorie Microwave ignited combustion synthesis of intermetallic compounds, modelling and experimental results, La Metallurgia Italiana 4 (2011).
[35] M.Y. Sandhu, A. Ali, I.C. Hunter, N.S. Roberts, A new method for the precise multiband microwave dielectric measurement using stepped impedance stub, Meas. Sci. Technol. 27 (2016), 117001, https://doi.org/10.1088/0957-0233/27/11/117001.
[36] S.M. Abdel-Samad, A.A. Fahmy, A.A. Massoud, A.M. Elbedwehy, Experimental investigation of TiO2-water nanofluids thermal conductivity synthesized by sol-gel technique, Curr. Nanosci. 13 (2017), https://doi.org/10.2174/1573413713666170619124221.
[37] M. Sadeghzadeh, H. Maddah, M.H. Ahmadi, A. Khadang, M. Ghazvini, A. Mosavi, N. Nabipour, Prediction of thermo-physical properties of TiO2-Al2O3/water nanoparticles by using artificial neural network, Nanomaterials 10 (2020) 697, https://doi.org/10.3390/NANO10040697.
[38] E.N. Gubareva, V.v. Strokova, Y.N. Ogurtsova, P.S. Baskakov, L.P. Singh, Composition and properties of TiO2 sol to produce a photocatalytic composite material, Key Eng. Mater. 854 (2020) 45–50, https://doi.org/10.4028/WWW.SCIENTIFIC.NET/KEM.854.45.
[39] L. Li, Y. Fang, Q. Xiao, Y.J. Wu, N. Wang, X.M. Chen, Microwave dielectric properties of fused silica prepared by different approaches, Int. J. Appl. Ceram. Technol. 11 (2014) 193–199, https://doi.org/10.1111/J.1744-7402.2012.02846.X.
[40] Z. Zhao, X. Shen, H. Li, K. Liu, H. Wu, X. Li, X. Gao, Watching microwave-induced microscopic hot spots via the thermosensitive fluorescence of europium/terbium mixed-metal organic complexes, Angew. Chem. 134 (2022), https://doi.org/10.1002/ANGE.202114340 e202114340.
[41] S. Horikoshi, A. Osawa, M. Abe, N. Serpone, On the generation of hot-spots by microwave electric and magnetic fields and their impact on a microwave-assisted heterogeneous reaction in the presence of metallic Pd nanoparticles on an activated carbon support, J. Phys. Chem. C 115 (2011) 23030–23035, https://doi.org/10.1021/JP2076269/ASSET/IMAGES/LARGE/JP-2011-076269_0006.JPEG.
[42] J. Wojnarowicz, T. Chudoba, A. Majcher, W. Łojkowski, Microwaves applied to hydrothermal synthesis of nanoparticles. Microwave Chemistry, De Gruyter, 2017, pp. 205–224, https://doi.org/10.1515/9783110479935/PDF.